Chemical routes to materials

Preparation of MoS$_2$ nanosheets to support Pd species for selective steerable hydrogenation of acetylene

Yang Guo[1], Jinlian Xie[2], Lijuan Jia[3,*] (ORCID), Yuzhen Shi[2], Jian Zhang[2], Qiuling Chen[2], and Qingqing Guan[2]

[1] Key Laboratory of Thermo-Fluid Science and Engineering, Ministry of Education, School of Energy and Power Engineering, Xi'an Jiaotong University, Xi'an 710049, Shaanxi, People's Republic of China

[2] Faculty of Environmental Science and Engineering, Kunming University of Science and Technology, Kunming 650500, People's Republic of China

[3] School of Chemistry and Environment, Yunnan Minzu University, Kunming 650500, People's Republic of China

ABSTRACT

Selective hydrogenation of acetylene to ethylene while avoiding over-hydrogenation into ethane is challenging for polymer industry. For highly steerable catalyst design of Metal-MoS$_2$, we reported a few-layer nano-MoS$_2$ supported Pd catalyst, in which the support was prepared by the exfoliation method of bulk molybdenum disulfide (MoS$_2$) in formamide solution. The results from TEM, SAED, AFM and Raman spectra analysis confirmed that the few-layer nano-MoS$_2$ was produced successfully. The XPS result indicates Pd charge transferred to MoS$_2$, proving strong Pd-MoS$_2$ interactions. Pd/nano-MoS$_2$ provided a good catalytic performance for the hydrogenation of acetylene to ethylene, and the ethylene selectivity can reach up to 75% while acetylene conversion can achieve nearly 100%. Comparing with the commercial 5% Pd/C catalyst reported at similar conditions, the Pd/nano-MoS$_2$ synthesized in this study presents better activity and selectivity. In all, this work shows potential application of MoS$_2$ nanosheets used as catalyst support to achieve selective steerable reactions.

Introduction

Hydrogenation of acetylene is one of typical and important reactions for polymer industry. The key is to convert acetylene to ethylene while avoid over-hydrogenation of ethylene into ethane [1]. Currently,

Pd-based catalysts are the most industrially used materials for selective hydrogenation of acetylene. Supports with high surface area are commonly employed to avoid agglomeration of Pd particles. Strong metal-support interactions can make some changes in catalytic properties of Pd catalysts to

Handling Editor: Annela M. Seddon.

Springer

achieve high ethylene selectivity [2, 3]. With the new material development, thus, there is still room for seeking novel catalyst supports for high selective hydrogenation of acetylene reaction.

Recently, nanoscale molybdenum disulfide (MoS$_2$) has attracted ever-growing interests in catalysis field due to good properties such as higher surface area, stronger adsorption ability and reactivity [4]. Compared with bulk MoS$_2$, nanoscale MoS$_2$ can either perform alone as a highly efficient catalyst or be used as a catalyst support material [5]. Previous studies have shown that the prepared nano-MoS$_2$ has two kinds of features: structural defects and complete structure [6, 7]. Coordination unsaturated edge atoms produced on the structural defects can provide enough active sites. This kind of MoS$_2$ nanosheets is mostly used as catalysts, but Nano-MoS$_2$ with multidegree of structural defects have somehow difficulties for application due to less stability [8]. MoS$_2$ nanosheets with complete crystal structure have higher atomic exposure rate on the base surface, resulting more edge atoms, more stable and non-agglomerative properties. Thus, it not only has better catalytic performance, but also potential to be used as a catalyst support [4].

Synthesizing complete structural nanoscale MoS$_2$ still remains a strenuous task. The major methods to produce nanoscale MoS$_2$ include mechanical exfoliation [9], chemical exfoliation [10, 11] or the combination of chemical and physical growth [12]. The lithium intercalation method in chemical exfoliation [13] and chemical vapor deposition [14] can prepare a large number of few- or mono-layers MoS$_2$ nanosheets, but with structural defects. The nano-MoS$_2$ prepared by hydrothermal method [15, 16] is mostly amorphous, and its internal structure is incomplete and results in many defects. Smith et al. [6] developed a reaction solution system equivalent to the surface energy of MoS$_2$ by adding sodium dodecyl sulfate (SDS) surfactant, which rapidly prepared two-dimensional nano-MoS$_2$ with complete structure under liquid-phase binding mechanical force (ultrasound). The results strongly proved that a few layers of MoS$_2$ nanosheets with complete structure can be achieved by liquid-phase exfoliated method, while some exfoliated solvents, e.g., N-methyl-2-pyrrolidone (NMP), isopropanol (IPA), dimethylformamide (DMF), effectively prevented the aggregation [17, 18]. Some solvents used for liquid-phase exfoliation have the properties of cheapness, good dispersibility and

strong stability. For instance, isopropyl alcohol (IPA), and aqueous ammonia (NH$_3$) have been found to be favorable for exfoliation of MoS$_2$ [19, 20]. Additionally, Huang et al. also found that with NMP assisted by formamide can enhance the exfoliation efficiency [20]. Therefore, it is potential to use formamide to exfoliate bulk MoS$_2$ for well-structured MoS$_2$ nanocatalyst support.

Herein, a new process of formamide solvent-assisted ultrasonic exfoliation of bulk MoS$_2$ was developed to prepare few-layer nano-MoS$_2$-based catalyst support with a well-structured nanosheet. The microbubble N$_2$ was used to enhance the impact force through the process of rapid enlargement and closing shrinkage under the action of ultrasonic field. We further tested the metal-MoS$_2$ interactions experimentally for selective hydrogenation of acetylene. In addition, a series of characterizations of the products (such as SEM, TEM, AFM, etc.) were carried out. The findings in this work are expected to be useful for further application of few-layer nano-MoS$_2$ for highly steerable design of catalysis systems.

Experiments

Materials

Chemical reagents used were of analytic grade. None of the reagents were treated with special treatment. The nitrogen is highly pure. MoS$_2$ (Sinopharm Chemical Reagent Co. Ltd, 98%) was purchased in powder form. All of the glassware were cleaned and reused after treatment with V_{HNO3}: V_{HCL} = 1:3. During the experiment, the deionized water (Milli-Q, Millipore) was used.

Preparation of nano-layer MoS$_2$

300 mg of MoS$_2$ was added into 40 mL of formamide solution (Damao chemical reagent factory) and filled the nitrogen. The mixture was sonicated (SB2200-T, Branson Ultrasonics (shanghai) Co. Ltd) for 8 h in ice-water bath. Afterward, the mixture was centrifuged at 4000 rpm for 30 min to collect supernatant. Furthermore, the top dispersion was centrifuged at 8000 rpm for 30 min to discard the unexfoliated flakes. Then, the supernatant centrifuged again at 12,000 rpm for 30 min. The process was repeated for several times until the supernatant became light-

colored. The final sediment MoS$_2$ nanosheets were obtained.

Preparation of catalyst

The MoS$_2$ nanosheets supported Pd catalysts applied in this work, were prepared according to the ethylene glycol reduction method, as previously reported [21]. Ethylene glycol was used as solvent and reducing agent. The detail process is as follows: 0.85 g MoS$_2$ nanosheets and 1.5 g PVP (Polyvinyl Pyrrolidone) were added to boiling flask-3-neck filled with 200 ml of ethylene glycol. After sonicating and stirring at room temperature, MoS$_2$ nanosheets were impregnated with palladium nitrate solution (12.36 mg) by magnetic stirring, subsequent adding sodium hydroxide (9 mg). Then the mixture was placed into an oil bath at 463 K and reduced for 4 h with continuous magnetic stirring. Finally, the mixture was washed and filtered with equal volume of ethanol. Then, we dried catalyst at 333 K for 10 h. Finally, 0.87 wt % Pd/MoS$_2$ nanosheets were prepared, which was detected by inductively coupled plasma (ICP) with an IRIS Interpid (II) XSP and NU AttoM.

Catalytic performance evaluation

Selective hydrogenation of acetylene was performed by a continuous flow fixed-bed stainless steel micro reactor over prepared Pd/MoS$_2$ nanosheets catalyst. 100 mg of the catalyst was reduced with flowing 20 vol % H$_2$/N$_2$ (20.4 mL min^{-1}) at 358 K for 1 h prior to use in the reaction. After the sample was cooled to room temperature, a gas mixture with a space velocity of 40,000 mL h^{-1} g^{-1} was introduced into the reactor, simulating the frontend hydrogenation conditions with 20.0 vol % C$_2$H$_2$ and 20.0 vol % H$_2$ balanced with He at a fixed H$_2$/acetylene ratio of 2. Mass flow controllers were used to control all gas flows. The reaction temperature was held constant for 20 min before ramping to the next temperature point. Reactant and reaction products were analyzed by gas chromatograph (GC7890A, Agilent, USA) with a thermal conductivity detector (TCD), which equipped a long silica packed column (Φ0.25 mm * 50 mm, Al$_2$O$_3$/Na$_2$SO$_4$ coating). The conversion and selectivity were calculated as:

$$\text{Conversion} = \frac{C_{C_2H_2(\text{inlet})} - C_{C_2H_2(\text{outlet})}}{C_{C_2H_2(\text{inlet})}} \times 100\% \quad (1)$$

$$\text{Selectivity} = \frac{C_{C_2H_2(\text{outlet})}}{C_{C_2H_2(\text{inlet})} - C_{C_2H_2(\text{outlet})}} \times 100\% \quad (2)$$

Characterization

Atomic force microscopy (AFM) was used to characterize the morphology of the nanosheets. The suspension was deposited on fresh mica by spin coating and dried under ambient condition. AFM (Bruker Multimode 8, German) was used to obtain images in a tapping mode using Olympus AC240TS probe. Transmission electron microscope (JEM-2100F, Japan) was observed at an accelerating voltage of 200 kV. The surface morphology was examined by a field-emission scanning electron microscopy (FEI PHILIPS XL-30). Raman spectroscopy was performed using in Via-Reflex with 536 nm excitation laser in air under ambient conditions. Ultraviolet Visible (UV–visible) spectroscopy was carried out to analyze the concentration of exfoliated MoS$_2$ with a Cary 60 spectrometer. The excitation wavelength is 532 nm. The gas components from the micro-reactor outlet were analyzed by online gas chromatography (Agilent Technologies 7820A GC system) equipped with an TCD detector.

Results and discussion

Characterization of nano-MoS$_2$

The suspensions of highly disperse few-layer MoS$_2$ sheets were prepared from body powder (Fig. 1a) by formamide exfoliation. The concentration of suspensions decreases with the increase of centrifugal rate (Fig. 1b), and the final concentration of MoS$_2$ nanosheets is about 0.15 mg/mL after 16,000 rpm centrifugation. Most few-layer MoS$_2$ sheets were obtained in this suspension and were further used as the supports for steerable hydrogenation of acetylene.

To explore the microstructure and quality of the exfoliation MoS$_2$ nanosheets, TEM analysis was carried out. The TEM images shown in Fig. 1c, d illustrate the two-dimensional ultrathin sheets individually disperse in the solution, showing that the typical piece morphologies of MoS$_2$ nanosheets. High-resolution TEM images are shown in Fig. 1 e, f.
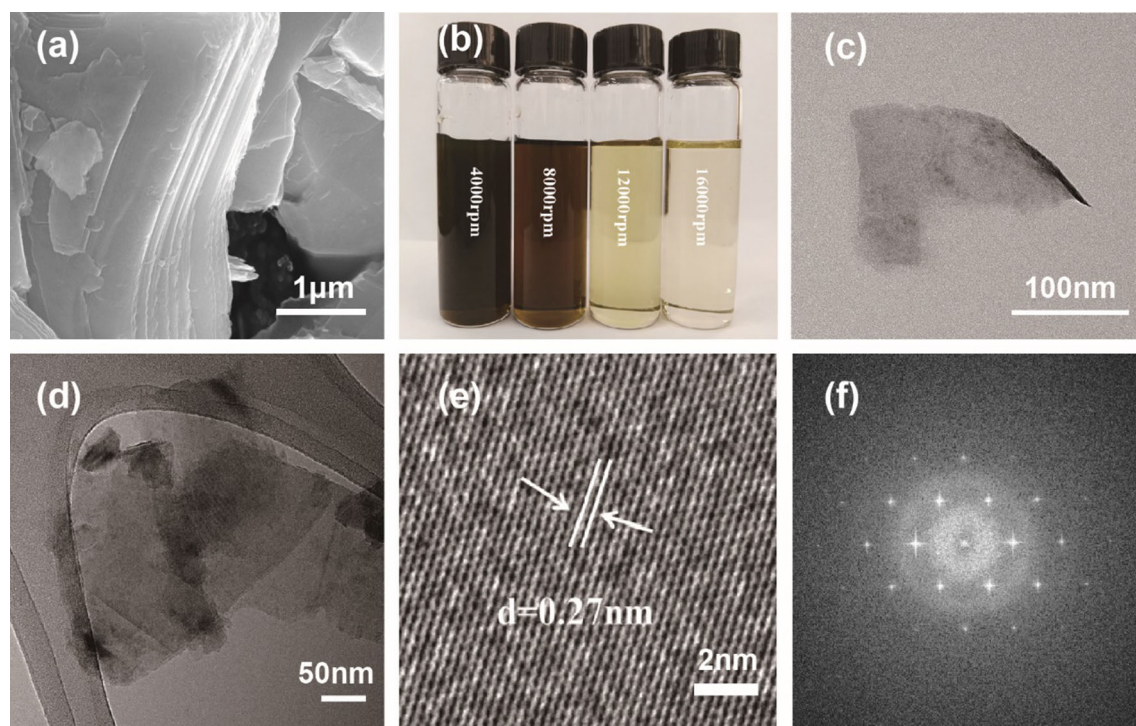
Figure 1 **a** Scanning electron microscopy image of MoS$_2$ powder. **b** Photograph of liquid-phase exfoliated MoS$_2$ suspension in formamide under different centrifugal rate. **c** ∼ **f** are TEM images of MoS$_2$ nanosheets. (**c** and **d**) Low-resolution TEM images of MoS$_2$ nanosheets. **e** High-resolution TEM images of MoS$_2$ sheets. **f** The selected area electron diffraction (SAED) patterns of image of few-layer MoS$_2$ sheets.

The lattice spacing was measured to be about 0.27 nm (Fig. 1e). It refers to fringe spacing of few-layer MoS$_2$ sheets (100 planes) [22]. The morphology of the MoS$_2$ nanosheets can be observed and their lateral sizes are typically in the range of 150 to 300 nm. The selected area electron diffraction (SAED) was also obtained. The typical hexagonal symmetry of the obtained MoS$_2$ nanosheets is consistent with the typical hexangular atomic structure of MoS$_2$ [10], indicating that the crystallinity is not damaged during the exfoliation process. It is advantageous to compare with MoS$_2$ exfoliated by lithium intercalation, which will result in substantial deviation from the original hexagonal structure [23]. Thus, formamide exfoliation can produce well-structured nano-MoS$_2$.

In order to further determine the size and thickness of MoS$_2$ nanosheets, AFM imaging was performed for height analysis at multiple locations across the most representative regions in the sample. The AFM topographic images shown in Fig. 2 are consistent with TEM results. The apparent height of MoS$_2$ nanosheets is found to be 1.2 ∼ 1.8 nm,

corresponding to 3–4 layers of MoS$_2$ [6]. The objects observed are hundreds of nanometers wide, in agreement with the SEM data. It is clear that the MoS$_2$ was exfoliated into individual layers. Therefore, the formamide system is promising to exfoliate the bulk MoS$_2$ for well-structured crystal structure nano-MoS$_2$.

Since 3–4 layers of MoS$_2$ show low XRD patterns with high background peaks, therefore the prepared liquid-phase exfoliated MoS$_2$ nanosheets were alternatively characterized by using Raman spectroscopy, and the result is demonstrated in Fig. 3. In a comparison of the exfoliated and bulk MoS$_2$ samples, the latter shows bands at 376 (E1 2 g) and 401 (A$_{1g}$) cm^{-1}, while the few-layered MoS$_2$ exhibits the corresponding bands at 383 and 408 cm^{-1}. Comparing with Li and co-workers' results [23], the peaks have higher frequency in the exfoliated material. The shift in the frequency of the A$_{1g}$ mode as a function of thickness indicates a transition from surface to bulk layers [24]. The intensities of the bands become significantly weaken, revealing that the number of layer decrease. Given the intensity of the full-widths at half

Figure 2 AFM image of **a** MoS$_2$ nanosheets, **b** height profiles of MoS$_2$ nanosheets, **c** AFM height analysis of the image.
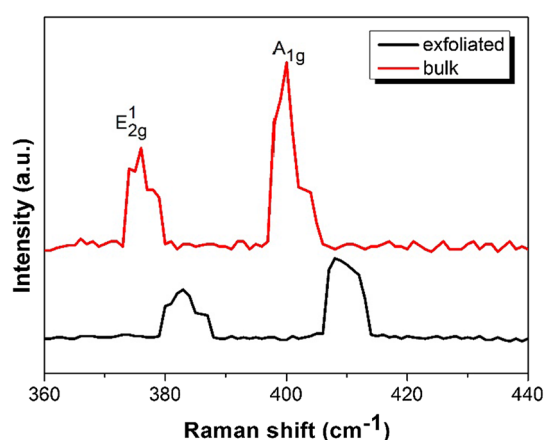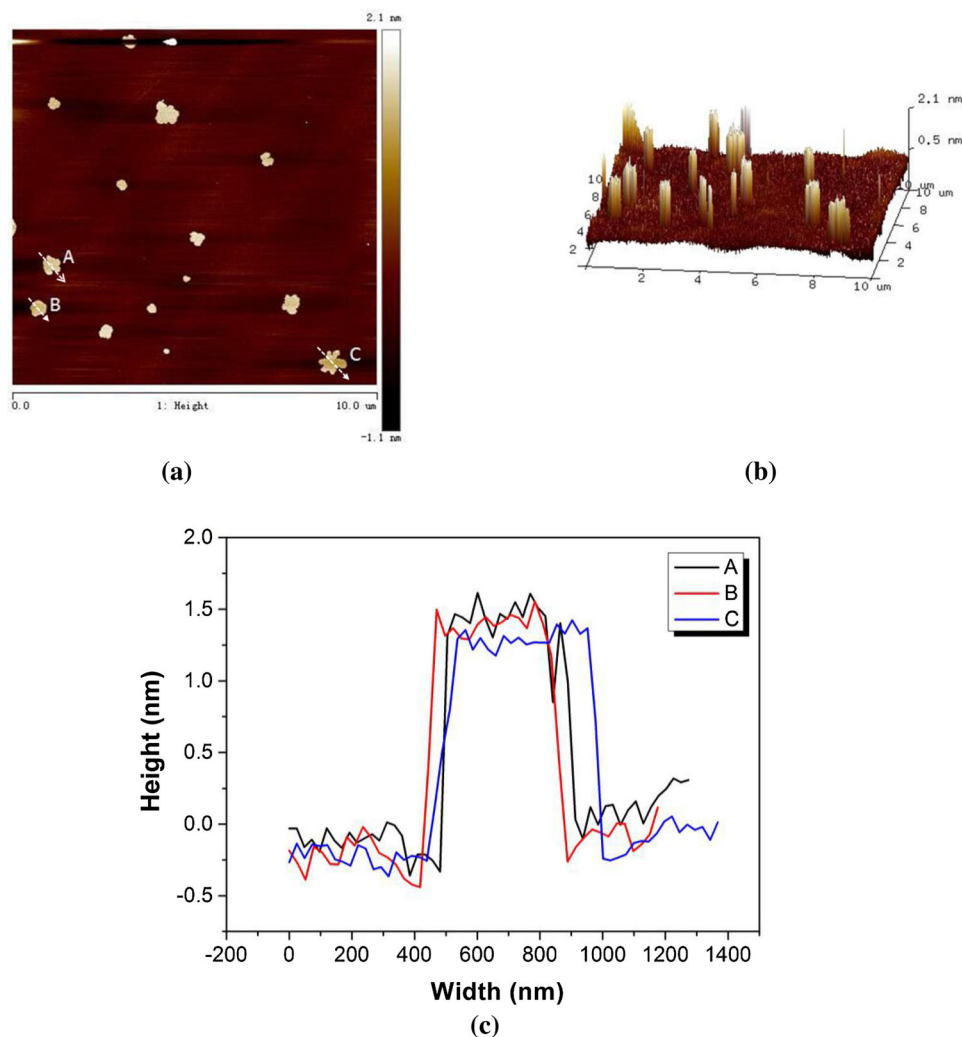

(a)

(b)

(c)

Figure 3 Raman spectra recorded using a 536 nm laser.

maximum values are obviously increased in the obtained products than that in the bulk samples, the

few-layers nano-MoS$_2$ has been synthetized successfully.

Characterization of Pd/nano-MoS$_2$

We further loaded about 0.87wt% Pd on the prepared few-layers nano-MoS$_2$. Due to the high dispersion or low concentration of Pd in the samples, XRD patterns did not find the peak of palladium. Thus, instead, the electronic structures of the elements in Pd/MoS$_2$ nanocatalyst are probed by XPS.

Figure 4a shows total XPS spectra of the nanocatalyst, which confirms the Pd does exist on the few-layers nano-MoS$_2$, suggesting a successful synthesis of the Pd/MoS$_2$ catalyst. In Fig. 4b, c, d, the S 2p, Mo 3d and Pd 3d regions of the Pd/MoS$_2$ nanocatalyst are shown, respectively. The doublet of Mo^{4+} band at 229.7 eV and 232.9 eV in the Mo 3d region of XPS agree well with that of MoS$_2$ in the literature [25]. Mo,
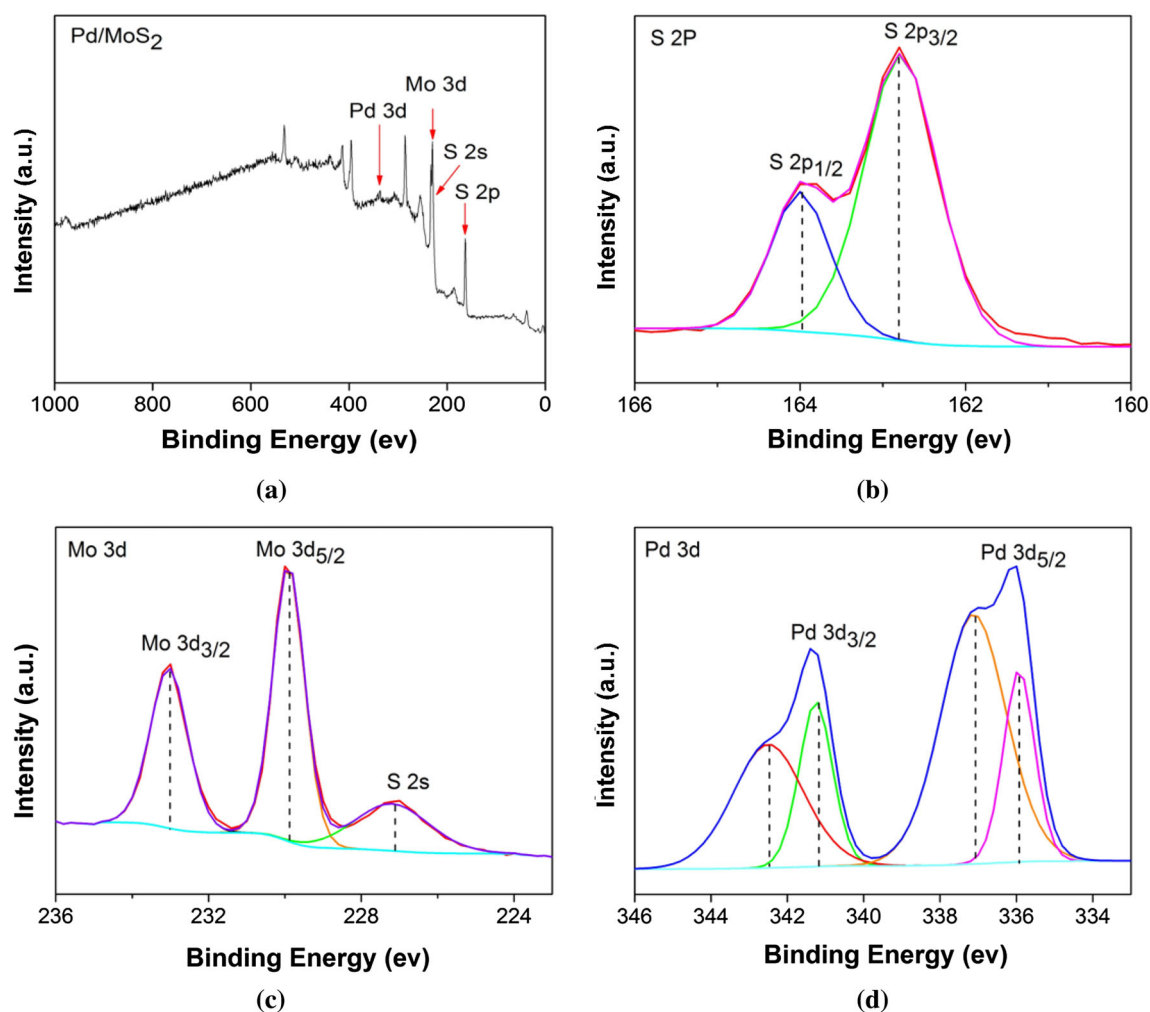
Figure 4 X-ray photoelectron spectra. **a** The whole region of Pd/MoS$_2$ nanocatalyst. **b** S 2p region and, **c** Mo 3d region of Pd/MoS$_2$, **d** Pd 3d region of catalyst.

Pd and S species also undergo changes in binding energy (BE) upon forming Pd/MoS$_2$ samples. The S 2p regions of the spectra show a twin peaks of S 2p$_{1/2}$ and S 2p$_{3/2}$ (Fig. 4b) at the corresponding BEs at 163.9 and 162.7 eV respectively. These can be assigned to S^{2-} in MoS$_2$, but are slightly blue-shifted from those of pure MoS$_2$ (S 2p$_{3/2}$ = 162.4 eV), suggesting charge transfer from Pd to MoS$_2$ [26]. The Pd 3d regions of the spectra are appeared to four sets of peaks as shown in Fig. 4d. The Pd 3d$_{5/2}$ peaks at 335.8 eV and 336.8 eV correspond to Pd^0 and Pd^{2+}, respectively [27]. Compared with metallic Pd (3d$_{5/2}$ = 335.1 eV), the peak assigned to Pd^0 is blue-shifted, implying charge transfer from Pd to MoS$_2$ [26]. Thus, strong Pd-nanoMoS$_2$ interactions do take place, suggesting promoted catalytic properties of Pd catalysts for acetylene hydrogenation.

Figure 5 demonstrates SEM and STEM images of Pd$_{0.87}$/MoS$_2$ nanocatalyst. As can be seen, Pd particles are scattered on glossy MoS$_2$ surface with low loading amount of Pd. To prove the existence of Pd particles, x-ray energy dispersive spectroscopy (EDS) was used. It is clear that Pd can be found. Thus, Pd$_{0.87}$/MoS$_2$ nanocatalyst was synthesized successfully.

Catalytic activity

The catalytic performance of the Pd/MoS$_2$ nanocatalyst was tested by acetylene selective hydrogenation experiment, and the results are shown in Fig. 6. We can see that, when the temperature is 80 °C, the conversion rate of acetylene reaches almost 100% at both 30,000 mL h^{-1} g^{-1} and 40,000 mL h^{-1} g^{-1}.
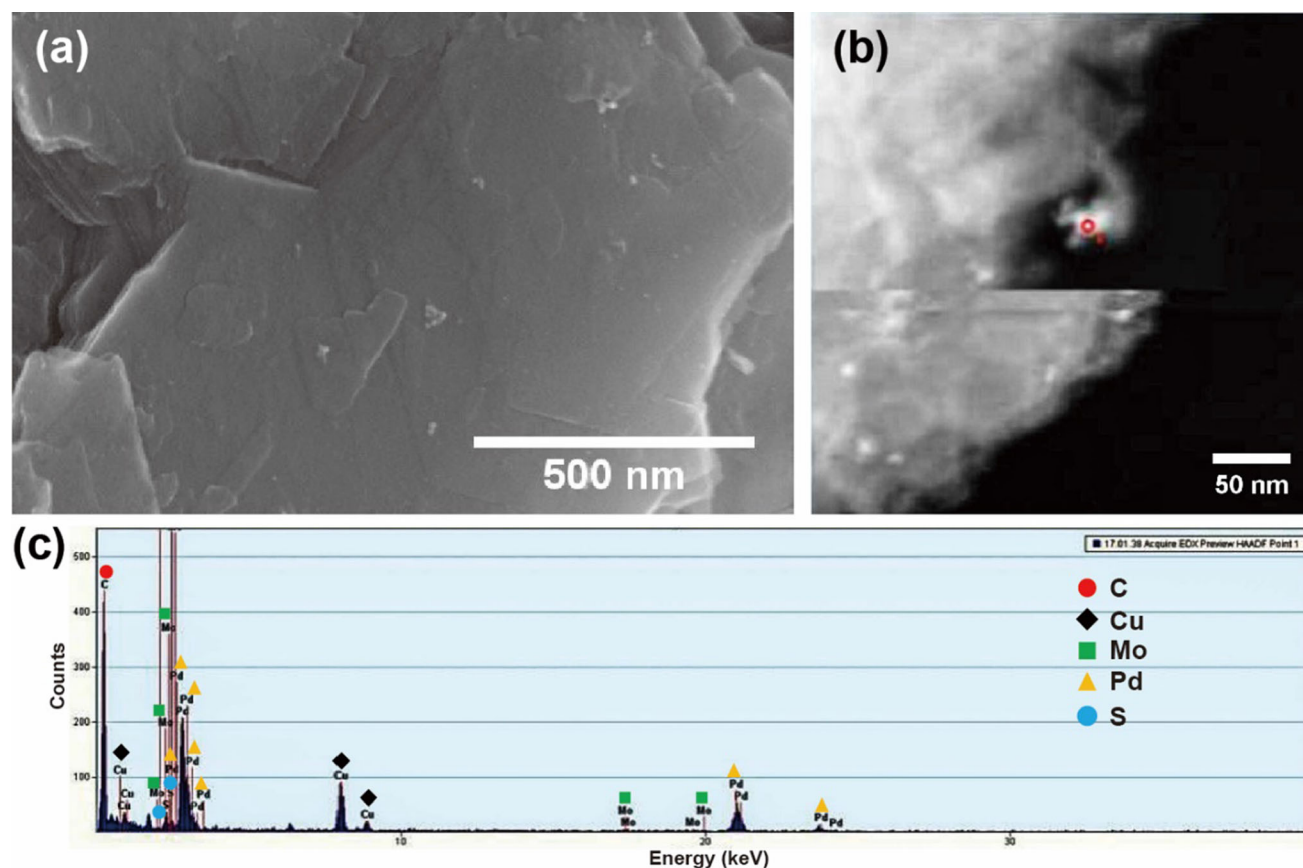
Figure 5 **a** SEM image, **b** STEM and **c** EDS of $Pd_{0.87}/MoS_2$ nanocatalyst.

Additionally, the ethylene selectivity at 40,000 mL h^{-1} g^{-1} is slightly higher than those of the 30,000 mL h^{-1} g^{-1}. This may be attributed to the increased adsorption of the catalyst on ethylene with the standing time, which was further converted. Either at 40,000 mL h^{-1} g^{-1} or 30,000 mL h^{-1} g^{-1}, under temperature approximately150 °C, the conversion efficiency and ethylene selectivity are the highest. In this occasion, the ethylene selectivity over the Pd/MoS_2 nanocatalyst reaches a maximum at ~75% with 100% acetylene conversion under 40,000 mL h^{-1} g^{-1}.

We also compared the selective hydrogenation of acetylene with the commercial catalyst 5% Pd/C from Sigma-Aldrich. The hydrogenation of acetylene with Pd/C can reach 100% under 40,000–80,000 mL h^{-1} g^{-1} at temperature 50–180 °C, but the ethylene selectivity is only about 15% at all conditions [21]. Thus, the metal-MoS_2 interactions decrease the hydrogenation activity and the adsorption of ethylene, leading high selective hydrogenation of acetylene toward ethylene. Additionally, it was

reported that 40–59% efficiency and 58–93% selectivity can be achieved by Pd/TiO_2 [28], ~ 65% efficiency and ~ 60% selectivity for Pd/SiO_2 [29], 100% efficiency and 71.27% selectivity for Pd/Al_2O_3 [30]. By comparison, Pd/nano-MoS_2 firmly shows good selectivity. Additionally, layer C_3N_4 was used to support Pd, 99% efficiency and 83% selectivity were found at ~ 110 °C [31], presenting similar high efficiency and selectivity as Pd/nano-MoS_2. Thus, it is potential to use few-layer nano-MoS_2 for highly steerable design of catalytic systems, especially for selective hydrogenation of acetylene toward ethylene.

Conclusions

In this paper, we have successfully prepared few-layer MoS_2 nanosheets through exfoliating the bulk MoS_2 by ultrasonication with formamide solution. It can obtain few hundred nanometers in size and 3–4 layers MoS_2 nanosheets and morphologies of MoS_2
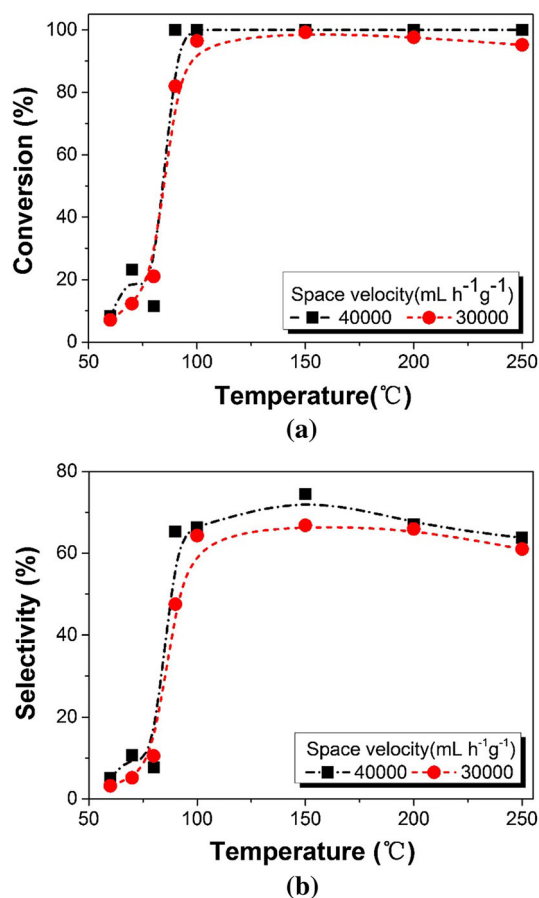
Figure 6 a Acetylene conversion and **b** ethylene selectivity versus reaction temperature over the $Pd_{0.87}/MoS_2$ nanocatalyst.

are schistose after exfoliation. The most few-layer MoS_2 sheets exist in the concentration of 0.15 mg/mL suspension and their perfect structures can be well retained. The MoS_2 nanosheets supported Pd catalyst provides high activity and ethylene selectivity during acetylene hydrogenation. Catalytic activity test results indicated that the ethylene selectivity over the Pd/MoS_2 nanosheets catalyst maintains at $\sim$75% with 100% acetylene conversion under 40,000 mL h^{-1} g^{-1}. SEM and STEM images testify that Pd particles are scattered on glossy MoS_2 surface with low loading amount of Pd. To prove, the X-ray energy dispersive spectroscopy (EDS) proved existence of Pd particles on the MoS_2 nanosheets. It is clear that Pd can be found. Thus, $Pd_{0.87}/MoS_2$ nanocatalyst was synthesized successfully. The XPS indicated Pd charge transfer from to MoS_2, proving the strong $Pd-MoS_2$ interactions. In all, it confirms our fabrication method for structurally complete and well-structured few-layer MoS_2 nanosheets and

provides potential application of MoS_2 nanosheets for supports to achieve selective steerable reactions.

Acknowledgements

References

[1] Nørskov JK, Bligaard T, Rossmeisl J, Christensen CH (2009) Nat Chem 1:37. https://doi.org/10.1038/nchem.121

[2] Tauster SJ, Fung SC, Baker RTK (1981) JA Horsley 211:1121. https://doi.org/10.1126/science.211.4487.1121

[3] Guan Q, Yang C, Wang S et al (2019) ACS Catal 9:11146. https://doi.org/10.1021/acscatal.9b04042

[4] Chhowalla M, Shin HS, Eda G, Li L-J, Loh KP, Zhang H (2013) Nat Chem 5:263. https://doi.org/10.1038/nchem.1589

[5] Tye CT, Smith KJ (2006) Catal Today 116:461. https://doi.org/10.1016/j.cattod.2006.06.028

[6] Coleman JN, Lotya M, O'Neill A et al (2011) Science 331:568. https://doi.org/10.1126/science.1194975

[7] Najmaei S, Yuan J, Zhang J, Ajayan P, Lou J (2015) Acc Chem Res 48:31. https://doi.org/10.1021/ar500291j

[8] Liu G, Robertson AW, Li MM-J et al (2017) Nat Chem 9:810. https://doi.org/10.1038/nchem.2740

[9] Li H, Wu J, Yin Z, Zhang H (2014) Acc Chem Res 47:1067. https://doi.org/10.1021/ar4002312

[10] Eda G, Yamaguchi H, Voiry D, Fujita T, Chen M, Chhowalla M (2011) Nano Lett 11:5111. https://doi.org/10.1021/nl201874w

[11] Ma H, Ben S, Shen Z et al (2020) Appl Surf Sci 512:145588. https://doi.org/10.1016/j.apsusc.2020.145588

[12] May P, Khan U, Hughes JM, Coleman JN (2012) J Phys Chem C 116:11393. https://doi.org/10.1021/jp302365w

[13] Yang F, Wang K, Hu P et al (2020) Appl Surf Sci 525:145867. https://doi.org/10.1016/j.apsusc.2020.145867

[14] Shi Y, Li H, Li L-J (2015) Chem Soc Rev 44:2744. https://doi.org/10.1039/C4CS00256C

[15] Chang K, Chen W, Ma L et al (2011) J Mater Chem 21:6251. https://doi.org/10.1039/C1JM10174A

[16] Lin X, Wang J, Chu Z et al (2020) Chin Chem Lett 31:1124. https://doi.org/10.1016/j.cclet.2019.07.003

[17] Lee K, Kim H-Y, Lotya M, Coleman JN, Kim G-T (2011) GS Duesberg 23:4178. https://doi.org/10.1002/adma.201101013

[18] Nguyen TP, Van Le Q, Choi KS et al (2015) Sci Adv Mater 7:700. https://doi.org/10.1166/sam.2015.1891

[19] Muscuso L, Cravanzola S, Cesano F, Scarano D, Zecchina A (2015) J Phys Chem C 119:3791. https://doi.org/10.1021/jp511973k

[20] Huang J, Deng X, Wan H et al (2018) ACS Sustain Chem Eng 6:5227. https://doi.org/10.1021/acssuschemeng.7b04873

[21] Jia L, Yu J, Chen Y et al (2017) J Supercrit Fluids 126:79. https://doi.org/10.1016/j.supflu.2017.02.017

[22] Xi Z, Erdosy DP, Mendoza-Garcia A et al (2017) Nano Lett 17:2727. https://doi.org/10.1021/acs.nanolett.7b00870

[23] Li H, Zhang Q, Yap CCR et al (2012) Adv Funct Mater 22:1385. https://doi.org/10.1002/adfm.201102111

[24] Lee C, Yan H, Brus LE, Heinz TF, Hone J, Ryu S (2010) ACS Nano 4:2695. https://doi.org/10.1021/nn1003937

[25] Acerce M, Voiry D, Chhowalla M (2015) Nat Nanotechnol 10:313. https://doi.org/10.1038/nnano.2015.40

[26] Li H, Yu K, Lei X, Guo B, Fu H, Zhu Z (2015) J Phys Chem C 119:22681. https://doi.org/10.1021/acs.jpcc.5b06729

[27] Drelinkiewicz A, Hasik M, Kloc M (2000) Catal Lett 64:41. https://doi.org/10.1023/A:1019078718474

[28] Kang JH, Shin EW, Kim WJ, Park JD, Moon SH (2002) J Catal 208:310. https://doi.org/10.1006/jcat.2002.3583

[29] Shin EW, Kang JH, Kim WJ, Park JD, Moon SH (2002) Appl Catal A 223:161. https://doi.org/10.1016/S0926-860X(01)00758-X

[30] Chen MH, Chu W, Dai XY, Zhang XW (2004) Catal Today 89:201. https://doi.org/10.1016/j.cattod.2003.11.027

[31] Huang X, Xia Y, Cao Y et al (2017) Nano Res 10:1302. https://doi.org/10.1007/s12274-016-1416-z